Journal of Alloys and Compounds 722 (2017) 48–53

Contents lists available at ScienceDirect

Journal of Alloys and Compounds

journal homepage: http://www.elsevier.com/locate/jalcom

# Enhanced emission of $Tm^{3+}$:$^3F_4 \rightarrow {}^3H_6$ transition by backward energy transfer from $Yb^{3+}$ in $Y_2O_3$ for mid-infrared applications

Dan Wu [a, b], Wenge Xiao [a, b], Xia Zhang [a], Zhendong Hao [a], Guo-Hui Pan [a], Liangliang Zhang [a], Yongshi Luo [a], Jiahua Zhang [a, *]

[a] State Key Laboratory of Luminescence and Applications, Changchun Institute of Optics, Fine Mechanics and Physics, Chinese Academy of Sciences, 3888 Eastern South Lake Road, Changchun, 130033, China
[b] University of Chinese Academy of Sciences, Beijing, 100049, China

ARTICLE INFO

*Article history:*
Received 7 March 2017
Received in revised form
28 May 2017
Accepted 7 June 2017
Available online 9 June 2017

*Keywords:*
2 μm emission
$Tm^{3+}$-$Yb^{3+}$
Backward energy transfer

ABSTRACT

$Tm^{3+}$ doped luminescence materials have attracted great attention owing to their potential for achieving 2 μm laser. Here, we report that the 2 μm emission intensity of $Tm^{3+}$:$^3F_4 \rightarrow {}^3H_6$ transition can be enhanced by as large as 1.8 times through introducing $Yb^{3+}$ into $Tm^{3+}$ doped $Y_2O_3$ upon 782 nm excitation, where the population of $Tm^{3+}$:$^3F_4$ level is increased by backward energy transfer from $Yb^{3+}$ following the forward energy transfer from the upper level $Tm^{3+}$:$^3H_4$ to an intermediate level $Yb^{3+}$:$^2F_{5/2}$. In addition, the efficiencies of $Yb^{3+}$ to $Tm^{3+}$ backward energy transfer are determined based on the analysis of emission spectra and fluorescence time profiles. It is found that the $Yb^{3+}$ to $Tm^{3+}$ backward energy transfer upon $Tm^{3+}$ excitation at 782 nm is more efficient than the $Yb^{3+}$ to $Tm^{3+}$ energy transfer upon $Yb^{3+}$ direct excitation at 980 nm, which is explained by the preferential excitation of $Yb^{3+}$ with a nearby $Tm^{3+}$ in the forward energy transfer from $Tm^{3+}$ to $Yb^{3+}$ upon $Tm^{3+}$ excitation. Our results demonstrate that codoping $Yb^{3+}$ into $Tm^{3+}$ activated materials offers a promising approach to obtain efficient 2 μm laser, and the efficient backward energy transfer may play a key role in other rare earth ions doped luminescence materials.



## 1. Introduction

Recently, great attention has been paid to the infrared lasers. Particularly, 2 μm lasers have received intense research for their potential applications including medicine, remote sensing and military technologies [1–7]. Among various rare earth (RE) ions who possess abundant levels, $Ho^{3+}$ and $Tm^{3+}$ are the most probable activators to generate 2 μm laser due to the transitions of $Ho^{3+}$:$^5I_7 \rightarrow {}^5I_8$ and $Tm^{3+}$:$^3F_4 \rightarrow {}^3H_6$ emissions [8–12]. The laser operation of $Ho^{3+}$ is limited because there is no available upper level in $Ho^{3+}$ to be excited from the ground level with the commercial 800 or 980 nm laser diodes. Therefore, the desirable 2 μm emission of $Ho^{3+}$ can be obtained only when the sensitizer $Yb^{3+}$ is codoped to provide efficient absorption at 980 nm [13–16]. As for $Tm^{3+}$, it has a reasonable absorption around 800 nm to be directly pumped by the available laser diodes and the broad emission about 300 nm allowing wide wavelength tuning [17,18].

For mid-infrared laser, an ideal host should possess low phonon energy to reduce multiphonon relaxation and thus increase the quantum efficiency. However, since resonant pumping cannot provide full population inversion and good signal-to-noise ratio, an upper level instead of the emitting level is pumped; therefore, populating the emitting level from the upper level becomes difficult owing to the slow multiphonon relaxation and the small branching ratio [19–21]. Accordingly, several RE ions such as $Pr^{3+}$, $Eu^{3+}$ and $Ce^{3+}$, have been used as the codopants to regulate the population [22–25]. For example, codoping $Ce^{3+}$ into $Er^{3+}$ activated luminescence augments the population of the $^4I_{13/2}$ level at the expense of that of the $^4I_{11/2}$ level due to the energy transfer from $Er^{3+}$($^4I_{11/2}$–$^4I_{13/2}$) to $Ce^{3+}$($^2F_{5/2}$–$^2F_{7/2}$), resulting in an enhancement of the 1550 nm emission to realize laser operation pumped by 980 nm [26,27]. The incorporation of $Ce^{3+}$ can also enhance the emission of $Ho^{3+}$:$^5I_7 \rightarrow {}^5I_8$ to obtain 2 μm laser [28,29]. Besides, Özen et al. [30–32] studied the blue upconversion emission of $Tm^{3+}$ under red light excitation at 683 nm in $Tm^{3+}$ and $Yb^{3+}$ codoped fluorophosphate glasses. They observed a considerable enhancement of the blue upconversion emission in the presence of

* Corresponding author.
*E-mail address:* zhangjh@ciomp.ac.cn (J. Zhang).

http://dx.doi.org/10.1016/j.jallcom.2017.06.088
0925-8388/

$Yb^{3+}$ due to the increased population of $^3F_4$ from which the blue level $^1G_4$ is reached by absorbing a red photon.

The sesquioxide $Y_2O_3$ is a suitable matrix for $RE^{3+}$ activated solid state lasers because of their excellent properties like good chemical stability, low thermal expansion and high thermal conductivity [33–35]. Moreover, it can be made into highly transparent ceramic with large sizes as well as good transparency even in the infrared region, which has been applied to obtain high power solid state lasers [36–38]. In addition, $Y_2O_3$ possesses relatively low phonon energy (phonon cutoff ≈ 591 $cm^{-1}$) [39], which is beneficial to the 2 μm emission of $Tm^{3+}$:$^3F_4$ → $^3H_6$ but also results in a relative low feeding to $^3F_4$ level upon 782 nm excitation. Generally, the population of $^3F_4$ level can be doubled due to the cross relaxation energy transfer ($^3H_4$, $^3H_6$) → ($^3F_4$, $^3F_4$) when the $Tm^{3+}$ concentration is high enough [17].

In the present work, we introduce $Yb^{3+}$ into $Tm^{3+}$ doped $Y_2O_3$ to enhance the 2 μm emission intensity of $Tm^{3+}$:$^3F_4$ → $^3H_6$ transition upon 782 nm excitation, in which the population of $^3F_4$ level is increased by the effect of $Tm^{3+}$-$Yb^{3+}$-$Tm^{3+}$ forward-backward energy transfer (FBET), i.e. the forward energy transfer (FET) from the upper level $Tm^{3+}$:$^3H_4$ to an intermediate level $Yb^{3+}$:$^2F_{5/2}$ and the subsequent backward energy transfer (BET) from $Yb^{3+}$ to $Tm^{3+}$ for populating the lower level of $Tm^{3+}$:$^3F_4$. Furthermore, the BET efficiencies from $Yb^{3+}$ to $Tm^{3+}$ in the FBET process are calculated based on the analysis of emission spectra and fluorescence time profiles. The results are also compared with the energy transfer efficiencies upon $Yb^{3+}$ direct excitation at 980 nm, indicating that the $Yb^{3+}$ to $Tm^{3+}$ backward energy transfer in FBET is more efficient than the $Yb^{3+}$ to $Tm^{3+}$ energy transfer upon $Yb^{3+}$ direct excitation at 980 nm. A preferential excitation of $Yb^{3+}$ with a nearby $Tm^{3+}$ in the FET process is proposed to explain the efficient $Yb^{3+}$ to $Tm^{3+}$ backward energy transfer.

## 2. Experimental

### 2.1. Sample preparation

The samples series of $(Y_{(1-x-y)}Tm_yYb_x)_2O_3$ ($x$ = 0–0.1, $y$ = 0.0005–0.01) powders were synthesized via the normal firing precursor method, which is considered to be more favorable to obtain uniform and highly crystallized samples than the traditional solid-state reaction. Typically, the appropriate amounts of $Y_2O_3$ (5N), $Tm_2O_3$ (5N) and $Yb_2O_3$ (6N) were first dissolved in dilute nitric acid (G.R.), respectively, to get the $Y(NO_3)_3$, $Tm(NO_3)_3$ and $Yb(NO_3)_3$ solutions. $Tm(NO_3)_3$, $Yb(NO_3)_3$ and $Y(NO_3)_3$ solutions were mixed stoichiometrically and stirred vigorously for 30 min at room temperature, and then dried at 95 °C for 24 h in a drying oven, followed by being preheated at 700 °C for 3 h to obtain the precursor. After grinding, the precursor was put into an alumina crucible and sintered at 1600°C for 5 h in air.

### 2.2. Measurements and characterization

The crystal structure of samples were characterized by X-ray diffraction (XRD) (Bruker D8 Focus diffractometer with Cu Kα radiation λ = 1.54056 Å). The emission spectra were measured using FLS920 spectrometer (Edinburgh Instruments, U.K.) in the wavelength range from 900 to 1700 nm. A 782 nm and a 980 nm laser diodes were used to pump $Tm^{3+}$:$^3H_4$ level and $Yb^{3+}$:$^2F_{5/2}$ level, respectively. The output excitation power density of 782 nm laser diodes was fixed at 35 mW/$mm^2$ while that of 980 nm laser diodes was fixed at 5 mW/$mm^2$. In fluorescence lifetime measurements, an optical parametric oscillator (OPO) was used as an excitation source and the signal was detected by a Tektronix digital oscilloscope (TDS 3052). All the measurements were carried out at room temperature.

## 3. Results and discussion

As shown in Fig. 1, the XRD patterns of $Tm^{3+}$ and/or $Yb^{3+}$ doped $Y_2O_3$ matches well with the JCPDS standard patterns of $Y_2O_3$ (PDF #41-1105), respectively. No impurity phase can be detected, indicating the formation of pure phase.

Fig. 2a and b show the emission spectra of $(Y_{0.9995-x}Tm_{0.0005}Yb_x)_2O_3$ with a fixed $Tm^{3+}$ concentration at 0.05 mol% and various $Yb^{3+}$ concentrations $x$ from 0 to 0.1 upon $Tm^{3+}$:$^3H_4$ excitation at 782 nm, respectively. In Fig. 2b, the emission intensity of $Tm^{3+}$:$^3F_4$ → $^3H_6$ transition in $Tm^{3+}$ singly doped sample is scaled to that in codoped sample. The emission spectra of the codoped samples consist of three emission bands around 900–1200 nm, 1350–1580 nm and 1580–1700 nm, which are assigned to $Yb^{3+}$:$^2F_{5/2}$ → $^2F_{7/2}$ transition, $Tm^{3+}$:$^3H_4$ → $^3F_4$ and $^3F_4$ → $^3H_6$ transitions, respectively. It should be noted that the peak around 1630 nm is only a part of $Tm^{3+}$:$^3F_4$ → $^3H_6$ emission (the complete emission is in the range of 1600–2200 nm) because the InGaAs detector used has a cutoff wavelength of 1650 nm. The appearance of $Yb^{3+}$ emission in the codoped samples indicates the existence of energy transfer from $Tm^{3+}$:$^3H_4$ level to $Yb^{3+}$:$^2F_{5/2}$ level. It is clear that the absolute intensity of $Tm^{3+}$:$^3F_4$ → $^3H_6$ emission in the codoped sample has a remarkable enhancement with increasing $x$ when compared with the $Tm^{3+}$ singly doped sample, and it increases by as high as 1.8 times at $x$ = 0.1(see Fig. 2a). This enhancement directly reflects the effect of the FBET processes, as shown in Fig. 3, which has been reported in $Er^{3+}$-$Yb^{3+}$ system as well [40]. To evaluate the efficiency of FBET, the efficiencies of both FET and BET should be known first.

The energy transfer efficiency can be calculated by

$$\eta = 1 - \frac{\tau}{\tau_0} \quad (1)$$

where $\tau_0$ and $\tau$ denote the excited state lifetimes of donor in the absence and in the presence of acceptor, respectively. To obtain $Tm^{3+}$:$^3H_4$ lifetimes, the fluorescence decay curves of $Tm^{3+}$:$^3H_4$ level are measured by monitoring the $Tm^{3+}$:$^3H_4$ → $^3H_6$ emission at

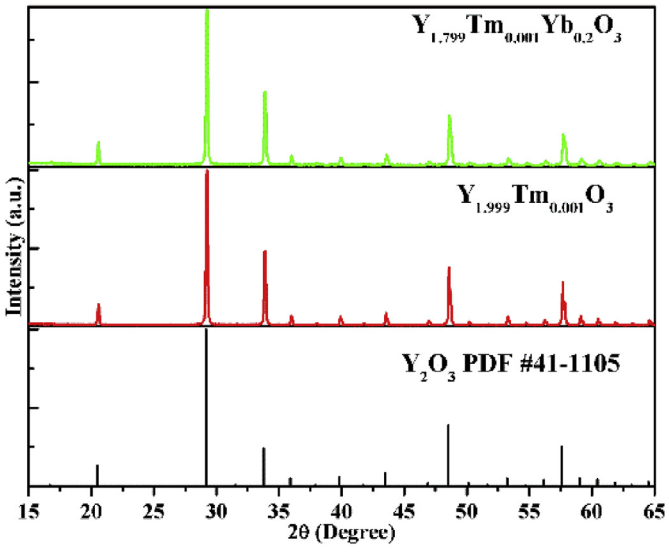


**Fig. 1.** The XRD patterns of $Tm^{3+}$ and/or $Yb^{3+}$ doped $Y_2O_3$, the standard pattern of $Y_2O_3$ (PDF #41-1105) is also presented for comparison.

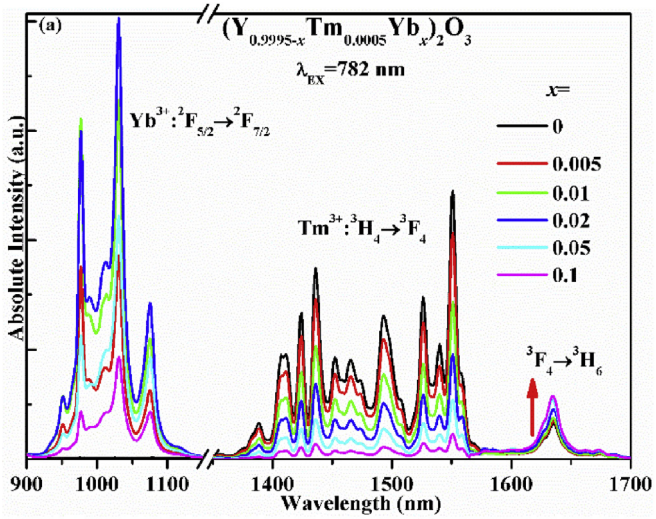


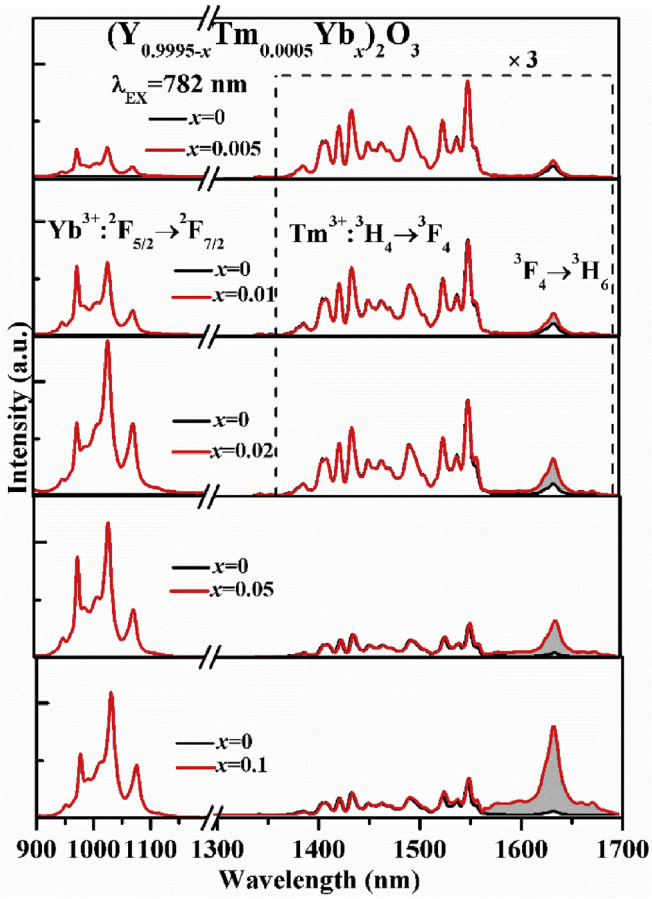


**Fig. 2.** a and b Emission spectra of $(Y_{0.9995-x}Tm_{0.0005}Yb_x)_2O_3$ ($x$ = 0.005–0.1) upon excitation to $Tm^{3+}$:$^3H_4$ level at 782 nm. The intensity of $^3H_4$ → $^3F_4$ emission in each spectrum is normalized in Fig. 2b.

811 nm under the excitation of $Tm^{3+}$:$^3F_3$ at 683 nm, as shown in Fig. 4. Using Eq. (1), the efficiencies of FET from $Tm^{3+}$ to $Yb^{3+}$ $\eta_{Tm\text{-}Yb}$ are calculated and listed in Table 1. It is exhibited that $\eta_{Tm\text{-}Yb}$ reaches 88% in $Y_2O_3$ for codoping with 10 mol% $Yb^{3+}$. In order to obtain the efficiency of BET from $Yb^{3+}$ to $Tm^{3+}$, $\eta_{Yb\text{-}Tm}$, it is necessary to study the dynamical processes for populating $Tm^{3+}$:$^3F_4$ level in the absence and in the presence of FBET. In the absence of FBET, for $Tm^{3+}$ singly doped sample, the $Tm^{3+}$:$^3F_4$ level is populated by $^3H_4$

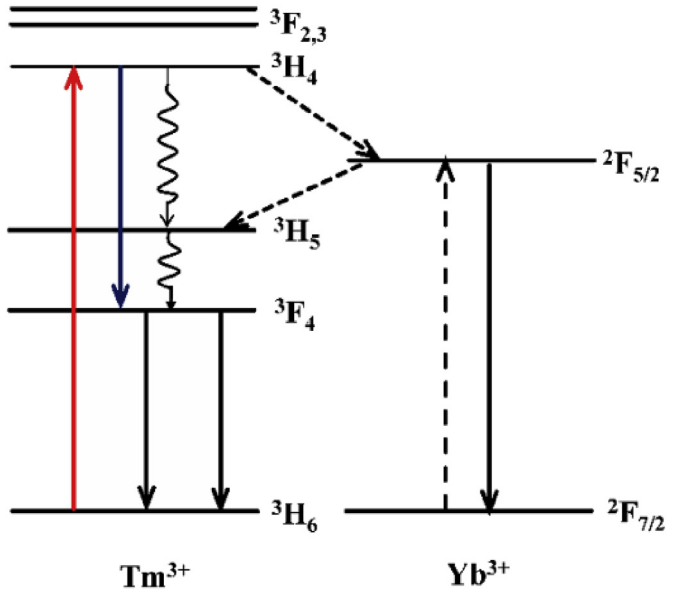


**Fig. 3.** Energy level diagrams and FBET process in $Tm^{3+}$ and $Yb^{3+}$ codoped crystal upon excitation to $Tm^{3+}$:$^3H_4$ level at 782 nm.

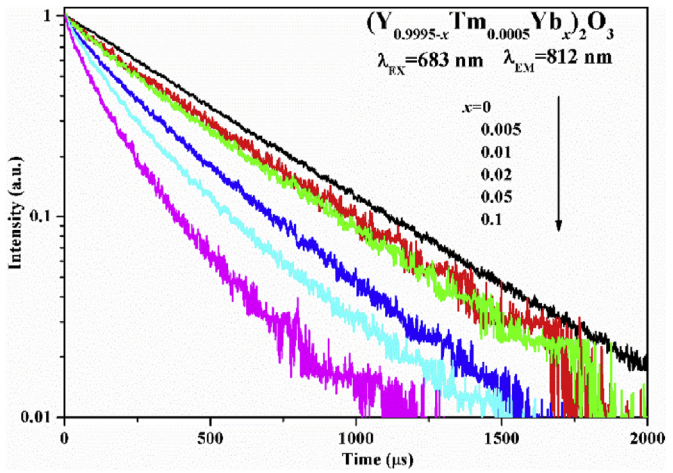


**Fig. 4.** Fluorescent decay curves of $Tm^{3+}$:$^3H_4$ level in $(Y_{0.9995-x}Tm_{0.0005}Yb_x)_2O_3$ ($x$ = 0.005–0.1) upon excitation to $Tm^{3+}$:$^3F_3$ level at 683 nm.

**Table 1**
The lifetimes of $Tm^{3+}$:$^3H_4$ level, and the efficiencies of FET, FET, BET and FBET in $(Y_{0.9995-x}Tm_{0.0005}Yb_x)_2O_3$ ($x$ = 0.005–0.1).

| $x$ | $Tm^{3+}$:$^3H_4$ (μs) $\lambda_{EX}$ = 683 nm $\lambda_{EM}$ = 812 nm | $\eta_{Tm\text{-}Yb}$ | $\eta_{Yb\text{-}Tm}$ | $\eta_{FBET}$ |
|---|---|---|---|---|
| 0 | 458 | | | |
| 0.005 | 397.7 | 0.13 | 0.82 | 0.11 |
| 0.01 | 343.3 | 0.25 | 0.74 | 0.19 |
| 0.02 | 359.5 | 0.43 | 0.79 | 0.34 |
| 0.05 | 126.7 | 0.72 | 0.90 | 0.65 |
| 0.1 | 57 | 0.88 | 0.88 | 0.77 |

level via intrinsic relaxation including multi-phonon relaxation (MPR) via $^3H_5$ level and the radiative transitions to $^3H_5$ or directly to $^3F_4$ levels. In other words, except the radiative transition to the ground state, all the rest of the population of $^3H_4$ level feeds the $^3F_4$

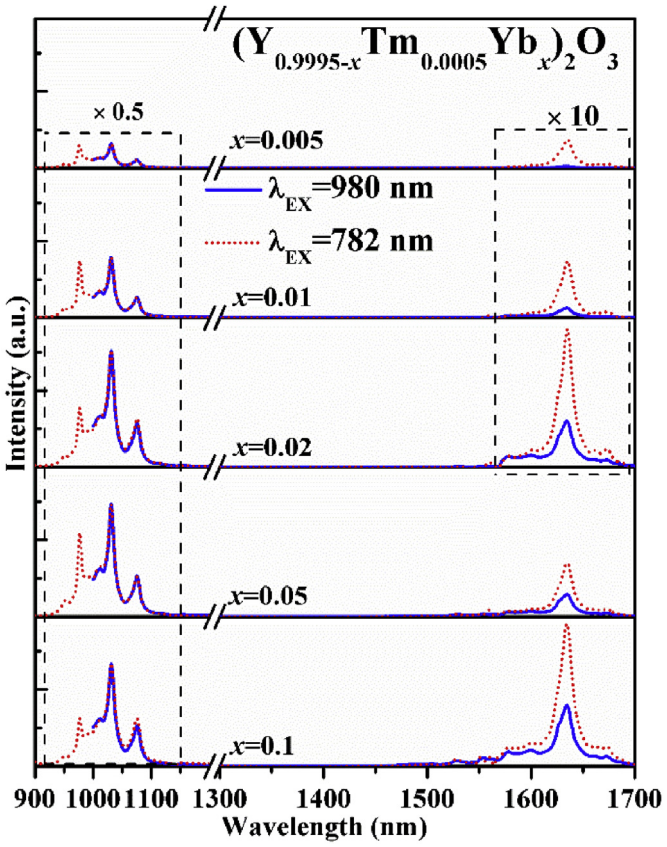


**Fig. 5.** Emission spectra of $(Y_{0.9995-x}Tm_{0.0005}Yb_x)_2O_3$ ($x$ = 0.005–0.1) upon 980 nm direct excitation to $Yb^{3+}$:$^2F_{5/2}$ level (solid). For comparison, the corresponding emission spectra upon excitation to $Tm^{3+}$:$^3H_4$ level at 782 nm (dotted) are also given. Note that the intensity of $Yb^{3+}$ emission upon 980 nm excitation is scaled to that upon 782 nm excitation.

level in the $Tm^{3+}$ singly doped sample. Note the cross relaxation (CR) process between two $Tm^{3+}$ ions, described as ($^3H_4$, $^3H_6$) → ($^3F_4$, $^3F_4$) [17], is neglected for populating the $^3F_4$ level since $Tm^{3+}$ concentration is fixed at as low as 0.05 mol% in this work. θ is defined as the ratio of the rate of intrinsic relaxation of $^3H_4$ → $^3F_4$ to the total rate of intrinsic decay of $^3H_4$ in $Tm^{3+}$ singly doped sample and thus it is reasonable to suppose θ is independent of $Yb^{3+}$ concentration. In the presence of FBET for the codoped samples, the origin of $Tm^{3+}$:$^3F_4$ → $^3H_6$ emission can be divided into two parts upon $^3H_4$ excitation. One is contributed by the intrinsic relaxation of $^3H_4$ → $^3F_4$ responsible for $Tm^{3+}$ singly doped sample (under the black line), denoted as $I_0$. The other is contributed by FBET responsible for the emission enhancement due to the effect of the codopant $Yb^{3+}$ (shaded area), denoted as $\Delta I$. The portion of $^3H_4$ population to populate the $^3F_4$ level via FBET process is then expressed as $\eta_{Tm\text{-}Yb}\eta_{Yb\text{-}Tm}$ and the $^3H_4$ population without undergoing FET is 1-$\eta_{Tm\text{-}Yb}$ of which θ(1-$\eta_{Tm\text{-}Yb}$) populates the $^3F_4$ level through intrinsic relaxation. Therefore, we have

$$\frac{\Delta I}{I_0} = \frac{\eta_{Tm-Yb}\eta_{Yb-Tm}}{\theta(1-\eta_{Tm-Yb})} \quad (2)$$

where $\Delta I/I_0$ can be obtained directly from the integral area under the emission spectra in Fig. 2b, θ is calculated to be 0.31 for $Y_2O_3$ (the calculation details are provided in Supporting Information). Using Eq. (2), $\eta_{Yb\text{-}Tm}$ in $Y_2O_3$ is calculated and listed in Table 1. One can find $\eta_{Yb\text{-}Tm}$ can reach 88% in $Y_2O_3$ when codoped with 10 mol% $Yb^{3+}$ although the concentration of $Tm^{3+}$ is as low as 0.05%. Accordingly, such highly efficient BET process makes the efficiency of FBET reach up to 77% in $Y_2O_3$ for codoping with 10 mol%$Yb^{3+}$. With regard to the efficient BET from $Yb^{3+}$ to $Tm^{3+}$, it is suggested that $Tm^{3+}$ prefers transferring energy to a nearby $Yb^{3+}$ in the forward process of FBET, thereby leading to the energy transfer from such excited $Yb^{3+}$ back to $Tm^{3+}$ efficiently, whereas the direct excitation of $Yb^{3+}$ at 980 nm gives equal probability to all $Yb^{3+}$ ions of which only a small fraction has a nearby $Tm^{3+}$ for a low concentration of $Tm^{3+}$ in this work.

To prove the above point, we further compared the intensity of $Tm^{3+}$: $^3F_4$ → $^3H_6$ emission contributed by BET from $Yb^{3+}$ to $Tm^{3+}$ in FBET upon $Tm^{3+}$:$^3H_4$ excitation at 782 nm with that upon $Yb^{3+}$:$^2F_{5/2}$ direct excitation at 980 nm. Fig. 5 shows the emission spectra of $(Y_{0.9995-x}Tm_{0.0005}Yb_x)_2O_3$ ($x$ = 0.005–0.1) upon 980 nm excitation (solid). The spectra of $Yb^{3+}$ emission as well as the incremental of $Tm^{3+}$:$^3F_4$ → $^3H_6$ emission due to the effect of FBET process upon 782 nm excitation obtained by spectral subtraction from Fig. 2b are also presented (dotted) for comparison, in which, for clarity, the intensity of the $Yb^{3+}$ emission upon 980 nm excitation is scaled to that upon 782 nm excitation. Upon 980 nm excitation, all the $Yb^{3+}$ ions are equally excited, and then, the energy transfer from $Yb^{3+}$ to $Tm^{3+}$ is a random process dominated by energy diffusion. One can readily find that the $Tm^{3+}$:$^3F_4$ → $^3H_6$ emission for 980 nm excitation is always weaker than that upon 782 nm excitation, especially for low doping level of $Yb^{3+}$. In both cases, since the $Tm^{3+}$:$^3F_4$ → $^3H_6$ emission is entirely due to the energy transfer from $Yb^{3+}$ to $Tm^{3+}$, the weaker $^3F_4$ → $^3H_6$ emission for 980 nm

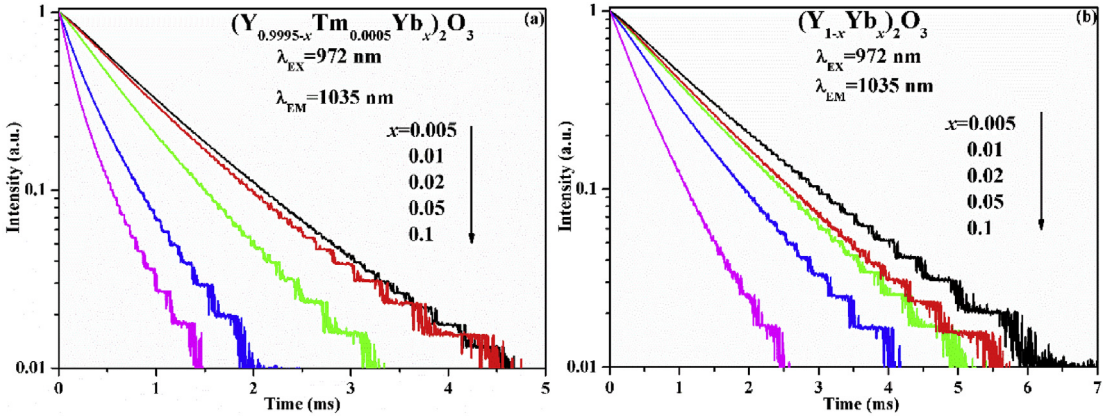


**Fig. 6.** Fluorescent decay curves of $Yb^{3+}$:$^2F_{5/2}$ level in $(Y_{0.9995-x}Tm_{0.0005}Yb_x)_2O_3$ ($x$ = 0.005–0.1) (a) and in $(Y_{1-x}Yb_x)_2O_3$ ($x$ = 0.005–0.1) upon excitation at 972 nm.

**Table 2**
The lifetimes of $Yb^{3+}$:$^2F_{5/2}$ level, the ratio $n$, BET efficiency $\eta_{Yb\text{-}Tm}$ and the normal energy transfer efficiency $\eta'_{Yb\text{-}Tm}$ in $(Y_{0.9995-x}Tm_{0.0005}Yb_x)_2O_3$ ($x = 0.005–0.1$).

| $x$ | $\tau_0$(μs) | $\tau$(μs) | $\eta'_{Yb\text{-}Tm}$ | $n$ | $\eta_{Yb\text{-}Tm}$ |
|---|---|---|---|---|---|
| | $\lambda_{EX}$ = 972 nm | $\lambda_{EX}$ = 972 nm | | | |
| | $\lambda_{EM}$ = 1033 nm | $\lambda_{EM}$ = 1033 nm | | | |
| 0.005 | 1240 | 886 | 0.29 | 13.9 | 0.85 |
| 0.01 | 1100 | 747 | 0.23 | 5.5 | 0.62 |
| 0.02 | 1030 | 616 | 0.40 | 3.0 | 0.67 |
| 0.05 | 810 | 308 | 0.62 | 2.4 | 0.80 |
| 0.1 | 440 | 188 | 0.57 | 2.9 | 0.80 |

excitation means lower transfer efficiency. If the intensity ratio of the $Tm^{3+}$:$^3F_4 \rightarrow {}^3H_6$ emission upon 782 nm excitation (dotted) to that upon 980 nm excitation (solid) is denoted by $n$, and the efficiency of energy transfer from $Yb^{3+}$ to $Tm^{3+}$ for 980 nm excitation is denoted by $\eta'_{Yb\text{-}Tm}$, then we have

$$n = \frac{\eta_{Yb-Tm}/(1-\eta_{Yb-Tm})}{\eta'_{Yb-Tm}/\left(1-\eta'_{Yb-Tm}\right)} \quad (3)$$

where $\eta'_{Yb\text{-}Tm}$ can be calculated using Eq. (1) with the fluorescence lifetimes $\tau_0$ and $\tau$ of $Yb^{3+}$ in the absence and in the presence of $Tm^{3+}$, respectively. To obtain the lifetimes of $Yb^{3+}$, the fluorescence decay curves of $Yb^{3+}$:$^2F_{5/2}$ level in $Yb^{3+}$ singly doped and codoped samples are upon 980 nm excitation, as shown in Fig. 6(a) and (b). The obtained fluorescence lifetimes of $Yb^{3+}$, $\eta'_{Yb\text{-}Tm}$ and $\eta_{Yb\text{-}Tm}$ calculated by Eq. (3) are listed in Table 2. Comparing Table 2 with Table 1, one can conclude that the values of $\eta_{Yb\text{-}Tm}$ calculated by Eq. (2) and that by Eq. (3) are consistent with each other. One may notice from Fig. 5 and Table 2 that the $n$ value decreases from 13.9 to 2.9 with $Yb^{3+}$ concentration increasing from $x = 0$ to $x = 0.1$. The above decrease indicates that the energy diffusion among $Yb^{3+}$ with the increase of $Yb^{3+}$ concentration is unavoidable and it weakens the selectivity between $Yb^{3+}$ and $Tm^{3+}$ in the backward energy transfer process. The increased energy diffusion goes against the effect of preferential excitation of $Yb^{3+}$ that followed by transferring to a nearby $Tm^{3+}$. Therefore, the backward energy transfer process is more effective in the lowly doping samples.

## 4. Conclusions

In summary, the emission intensity of $Tm^{3+}$:$^3F_4 \rightarrow {}^3H_6$ transition is enhanced by 1.8 times through introducing $Yb^{3+}$ into $Tm^{3+}$ doped $Y_2O_3$ upon 782 nm excitation, in which the population of $^3F_4$ level is increased by backward energy transfer from $Yb^{3+}$ following the forward energy transfer from the upper level $Tm^{3+}$:$^3H_4$ to an intermediate level $Yb^{3+}$:$^2F_{5/2}$. The FBET process in $(Y_{0.9995-x}Tm_{0.0005}Yb_x)_2O_3$ is investigated in detail as a function of $Yb^{3+}$ concentration. The BET efficiency is calculated to be as high as 88% for codoping with 10 mol% $Yb^{3+}$. The FBET process is also compared with the normal energy transfer process upon direct excitation to $Yb^{3+}$ at 980 nm, indicating that the BET is usually more efficient than the normal energy transfer, especially when the $Yb^{3+}$ concentration is relatively low, which is explained by the preferential excitation of $Yb^{3+}$ with a nearby $Tm^{3+}$ in the FET process. Our results demonstrate that $Yb^{3+}$ can act as an effective bridge between the upper and excitation level $^3H_4$ and the lower and emitting level $^3F_4$ of $Tm^{3+}$ to obtain efficient 2 μm emission. Furthermore, the efficient backward energy transfer that is in favor of the population of the lower energy level may also play a key role in other codoped luminescence materials.

## Acknowledgements

This work was partially supported by the National Key Research and Development Program of China (Grant No. 2016YFB0701003, 2016YFB0400605), National Natural Science Foundation of China (Grant No. 61275055, 11274007, 51402284 and 11604330), Natural Science Foundation of Jilin Province (Grant No. 20140101169JC, 20150520022JH and 20160520171JH), and the prior sci-tech program of innovation and entrepreneurship of oversea Chinese talent of Jilin province.

## Appendix A. Supplementary data

Supplementary data related to this article can be found at http://dx.doi.org/10.1016/j.jallcom.2017.06.088.

## References

[1] S. Kharitonov, C.S. Bres, Isolator-free unidirectional thulium-doped fiber laser, Light Sci. Appl. 4 (2015) e340.
[2] Q. Wang, J. Geng, S. Jiang, 2-μm fiber laser sources for sensing, Opt. Eng. 53 (2014), 061609.
[3] C.W. Rudy, M.J. Digonnet, R.L. Byer, Advances in 2-μm Tm-doped mode-locked fiber lasers, Opt. Fiber Technol. 20 (2014) 642–649.
[4] S.D. Jackson, Cross relaxation and energy transfer upconversion processes relevant to the functioning of 2 μm $Tm^{3+}$-doped silica fibre lasers, Opt. Commun. 230 (2004) 197–203.
[5] P. Koopmann, S. Lamrini, K. Scholle, P. Fuhrberg, K. Petermann, G. Huber, Efficient diode-pumped laser operation of Tm: Lu2O3 around 2 μm, Opt. Let. 36 (2011) 948–950.
[6] J. Yuan, W.C. Wang, D.D. Chen, M.Y. Peng, Q.Y. Zhang, Z.H. Jiang, Enhanced 1.8 μm emission in $Yb^{3+}$/$Tm^{3+}$ codoped tungsten tellurite glasses for a diode-pump 2.0 μm laser, J. Non-Cryst. Solids 402 (2014) 223–230.
[7] P. Camy, J.L. Doualan, S. Renard, A. Braud, V. Ménard, R. Moncorgé, $Tm^{3+}$: $CaF_2$ for 1.9 μm laser operation, Opt. Commun. 236 (2004) 395–402.
[8] G. Tang, X. Wen, Q. Qian, T. Zhu, W. Liu, M. Sun, X. Chen, Z. Yang, Efficient 2.0 μm emission in $Er^{3+}$/$Ho^{3+}$ co-doped barium gallo-germanate glasses under different excitations for mid-infrared laser, J. Alloy. Compd. 664 (2016) 19–24.
[9] S. Lamrini, P. Koopmann, M. Schäfer, K. Scholle, P. Fuhrberg, Efficient high-power Ho: YAG laser directly in-band pumped by a GaSb-based laser diode stack at 1.9 μm, Appl. Phys. B 106 (2012) 315–319.
[10] B. Huang, Y. Zhou, P. Cheng, Z. Zhou, J. Li, G. Yang, The 1.85 μm spectroscopic properties of $Er^{3+}$/$Tm^{3+}$ co-doped tellurite glasses containing silver nanoparticles, J. Alloy. Compd. 686 (2016) 785–792.
[11] A. Sidorowicz, A. Wajler, H. Węglarz, M. Nakielska, K. Orliński, R. Diduszko, A. Olszyna, Preparation and characterization of thulium doped yttrium oxide (Tm:$Y_2O_3$) powders, J. Alloy. Compd. 709 (2017) 293–298.
[12] J.H. Mun, A. Jouini, A. Novoselov, Y. Guyot, A. Yoshikawa, H. Ohta, H. Shibata, Y. Waseda, G. Boulon, T. Fukuda, Growth and characterization of Tm-doped $Y_2O_3$ single crystals, Opt. Mater. 29 (2007) 1390–1393.
[13] T. Zhu, G. Tang, X. Chen, M. Sun, Q. Qian, D. Chen, Z. Yang, 2 μm Fluorescence emission and energy transfer in $Yb^{3+}$/$Ho^{3+}$ Co-doped lead silicate glass, Int. J. Appl. Glass Sci. (2016) 1–8.
[14] T. Rothacher, W. Lüthy, H.P. Weber, Diode pumping and laser properties of Yb: Ho: YAG, Opt. Commun. 155 (1998) 68–72.
[15] G. Bai, L. Tao, K. Li, L. Hu, Y. Tsang, Enhanced~ 2μm and upconversion emission from Ho–Yb codoped oxyfluoride glass ceramics, J. Non-Cryst. Solids 361 (2013) 13–16.
[16] S. Balaji, A.D. Sontakke, R. Sen, A. Kalyandurg, Efficient~2.0 μm emission from $Ho^{3+}$ doped tellurite glass sensitized by $Yb^{3+}$ ions: judd-Ofelt analysis and energy transfer mechanism [Invited], Opt. Mater. Express 1 (2011) 138–150.
[17] D.C. Yu, R. Martín-Rodríguez, Q.Y. Zhang, A. Meijerink, F.T. Rabouw, Multi-photon quantum cutting in $Gd_2O_2S$: $Tm^{3+}$ to enhance the photo-response of solar cells, Light Sci. Appl. 4 (2015) e344.
[18] F. Esteban-Betegón, C. Zaldo, C. Cascales, Hydrothermal $Tm^{3+}$– $Lu_2O_3$ nanorods with highly efficient 2 μm emission, Inorg. Chem. 50 (2011) 2836–2843.
[19] F. Stutzki, C. Gaida, M. Gebhardt, F. Jansen, C. Jauregui, J. Limpert, A. Tünnermann, Tm-based fiber-laser system with more than 200 MW peak power, Opt. Let. 40 (2015) 9–12.
[20] B. D. Richards, C. A. Evans, Z. Ikonić, P. Harrison, Y. H. Tsang, D. J. Binks, J. Lousteau, A. Jha, Numerical rate equation modelling of a 1.61 μm pumped~ 2 μm Tm3+-doped tellurite fibre laser, In Photonics Europe 6998 (2008) 69981T International Society for Optics and Photonics.
[21] T. Sasikala, L.R. Moorthy, K. Pavani, T. Chengaiah, Spectroscopic properties of $Er^{3+}$ and $Ce^{3+}$ co-doped tellurite glasses, J. Alloy. Compd. 542 (2012) 271–275.
[22] Y. Tian, T. Wei, X. Jing, J. Zhang, S. Xu, Enhanced 2.7-and 2.9-μm emissions in $Er^{3+}$/$Ho^{3+}$ doped fluoride glasses sensitized by $Pr^{3+}$ ions, Mater. Res. Bull. 76 (2016) 67–71.

[23] A.F.H. Librantz, S.D. Jackson, F.H. Jagosich, L. Gomes, G. Poirier, S.J.L. Ribeiro, Y. Messaddeq, Excited state dynamics of the $Ho^{3+}$ ions in holmium singly doped and holmium, praseodymium-codoped fluoride glasses, J. Appl. Phys. 101 (2007), 123111.
[24] S. Shen, B. Richards, A. Jha, Enhancement in pump inversion efficiency at 980 nm in $Er^{3+}$, $Er^{3+}/Eu^{3+}$ and $Er^{3+}/Ce^{3+}$ doped tellurite glass fibers, Opt. Express 14 (2006) 5050–5054.
[25] Y.G. Choi, D.S. Lim, K.H. Kim, D.H. Cho, H.K. Lee, Enhanced $^4I_{11/2} \rightarrow {}^4I_{13/2}$ transition rate in $Er^{3+}/Ce^{3+}$ codoped tellurite glasses, Electron. Lett. 35 (1999) 1765–1767.
[26] C. Strohhöfer, A. Polman, Enhancement of $Er^{3+}$ $^4I_{13/2}$ population in $Y_2O_3$ by energy transfer to $Ce^{3+}$, Opt. Mater. 17 (2001) 445–451.
[27] F. Yang, B. Huang, L. Wu, Y. Zhou, F. Chen, G. Yang, J. Li, Enhanced 1.53 μm radiative transition in $Er^{3+}/Ce^{3+}$ co-doped tellurite glass modified by $B_2O_3$ oxide, Opt. Mater. 47 (2015) 149–156.
[28] T. Wang, F. Huang, W. Cao, Y. Guo, R. Lei, R. Ye, J. Zhang, S. Xu, Positive influence of $Ce^{3+}$ on effective transfer $Yb^{3+}$:$^7F_{5/2} \rightarrow Ho^{3+}$:$^5I_6$ in silica-germanate glass for mid-infrared applications, Opt. Mater. Express 7 (2017) 1084–1095.
[29] L. Tao, Y.H. Tsang, B. Zhou, B. Richards, A. Jha, Enhanced 2.0 μm emission and energy transfer in $Yb^{3+}/Ho^{3+}/Ce^{3+}$ triply doped tellurite glass, J. Non-Cryst. Solids 358 (2012) 1644–1648.
[30] G. Özen, J.P. Denis, P. Goldner, X. Wu, M. Genotelle, F. Pellé, Enhanced $Tm^{3+}$ blue emission in Tm, Yb, co-doped fluorophosphate glasses due to back energy transfer processes, Appl. Phys. Lett. 62 (1993) 928–930.
[31] X. Wu, J.P. Denis, G. Özen, P. Goldner, M. Genotelle, F. Pellé, The blue upconversion luminescence of vitroceramics codoped with $Tm^{3+}$ and $Yb^{3+}$ ions pumped with 680 nm, Chem. Phys. Lett. 203 (1993) 211–214.
[32] G. Ozen, J.P. Denis, M. Genotelle, F. Pelle, Tm-Yb-Tm energy transfers and effect of temperature on the fluorescence intensities in oxyfluoride tellurite compounds, J. Phys. Condens. Mat. 7 (1995) 4325.
[33] F. Vetrone, J.C. Boyer, J.A. Capobianco, A. Speghini, M. Bettinelli, Concentration-dependent near-infrared to visible upconversion in nanocrystalline and bulk $Y_2O_3$:$Er^{3+}$, Chem. Mater. 15 (2003) 2737–2743.
[34] C. Kränkel, Rare-earth-doped sesquioxides for diode-pumped high-power lasers in the 1-, 2-, and 3-μm spectral range, IEEE J. Sel. Top. Quant. 21 (2015) 250–262.
[35] P. Koopmann, S. Lamrini, K. Scholle, M. Schäfer, P. Fuhrberg, G. Huber, Holmium-doped $Lu_2O_3$, $Y_2O_3$, and $Sc_2O_3$ for lasers above 2.1 μm, Opt. Express 21 (2013) 3926–3931.
[36] C. Greskovich, J.P. Chernoch, Improved polycrystalline ceramic lasers, J. Appl. Phys. 45 (1974) 4495–4502.
[37] P.Y. Poma, K.U. Kumar, M.V.D. Vermelho, K. Serivalsatit, S.A. Roberts, C.J. Kucera, J. Ballato, L.G. Jacobsohn, C. Jacinto, Luminescence and thermal lensing characterization of singly $Eu^{3+}$ and $Tm^{3+}$ doped $Y_2O_3$ transparent ceramics, J. Lumin 161 (2015) 306–312.
[38] J. Lu, J. Lu, T. Murai, K. Takaichi, T. Uematsu, K.I. Ueda, H. Yagi, T. Yanagitani, A.A. Kaminskii, $Nd^{3+}$: $Y_2O_3$ ceramic laser, Jpn. J. Appl. Phys. 40 (2001) L1277.
[39] T. Sanamyan, J. Simmons, M. Dubinskii, Efficient cryo-cooled 2.7-μm $Er^{3+}$: $Y_2O_3$ ceramic laser with direct diode pumping of the upper laser level, Laser Phys. Lett. 7 (2010) 569–572.
[40] J. Zhang, Z. Hao, J. Li, X. Zhang, Y. Luo, G. Pan, Observation of efficient population of the red-emitting state from the green state by non-multiphonon relaxation in the $Er^{3+}$–$Yb^{3+}$ system, Light Sci. Appl. 4 (2015) e239.